Bull. Mater. Sci., Vol. 36, No. 6, November 2013, pp. 953–960. © Indian Academy of Sciences.

A novel method for massive synthesis of SnO_2 nanowires

GUODONG ZHANG and NIAN LIU*
Department of Materials Engineering, Wuhan University, Wuhan 430072, P. R. China

MS received 23 April 2012; revised 18 August 2012

Abstract. **This paper reports a simple, inexpensive and fast method to prepare SnO_2 nanowires. A large amount of ultra-long high purity single-crystalline SnO_2 nanowires with rutile structure, that is over hundreds of micrometers in length and 20–100 nm in diameter, have been synthesized through a one-step typical thermite reaction at 200 °C in O_2 atmosphere, with a gas pressure of 0·9 atm. These SnO_2 nanowires do not grow in one direction as those synthesized by other methods do, and are perfect single crystals without any dislocation or point defects detected in TEM images. The optoelectronic properties of these smooth and uniform nanowires have been characterized by means of X-ray photoelectron spectra, laser Raman spectrum and Fourier transform infrared spectrum. The result of X-ray photoelectron spectra analysis shows that some oxygen vacancies exist in these SnO_2 nanowires. In addition, possible growth mechanism of the SnO_2 nanowires has been described in detail by the studies of comparative experiments, which is quite different from that of SnO_2 nanowires synthesized by some other methods.**

Keywords. **SnO_2; nanowires; thermite reaction; growth mechanism.**

1. Introduction

One-dimensional SnO_2 materials, i.e. nanowires and nanorods, are of great interest for many applications due to their wide bandgap, special surface properties as well as unique electronic and optical properties (Ma *et al* 2004; Jin *et al* 2005; Salviati *et al* 2005; Jang *et al* 2006; Suhua *et al* 2006; Dmitriev *et al* 2007; Liu *et al* 2007; Mazzone 2007; Park *et al* 2007). The electronic and optical properties of SnO_2 nanowires can be improved by the addition of adequate doping materials (Huang *et al* 2007; Wan *et al* 2007; Bhise *et al* 2010). These excellent properties combined with high specific surface areas of SnO_2 nanowires make them widely used in gas sensors (Ahmad and Walsh 2003; Kang and Lee 2003; Pijolat *et al* 2003; Francisco *et al* 2008), transparent electrodes (Ito *et al* 2004), lithium-ion batteries (Ying *et al* 2005) and dye-sensitized solar cells (Gubbala *et al* 2008). SnO_2 nanowires were first synthesized in 2002 by a simple precursor thermal decomposition process in NaCl flux with $Sn(CO_3)_2$ as the precursor (Wang *et al* 2002). Zhou *et al* (2006) developed process for producing SnO_2 nanowires in a molten salt approach by using hydrothermal synthesized precursor and Wang *et al* (2008) simplified their original process to synthesize SnO_2 by oxidizing SnO nanoparticles in NaCl flux. Chemical vapour deposition has also been used to grow SnO_2 nanowires with diameters ranging from 30–80 nm (Calestani *et al* 2005; Qu *et al* 2007; Tae-Hwan *et al* 2008). At the same time, there were other considerable efforts devoted to the synthesis of SnO_2 nanowires, including thermal evaporation of SnO powder (Chen *et al* 2003; Jong-Soo *et al* 2004), carbothermal reduction process employing SnO as the starting material (Wang *et al* 2004; Budak *et al* 2006; Thanasanvorakun *et al* 2008), thermal oxidation of tin powder using gold film as the catalyst (Luo *et al* 2006), gas-reaction method (Jian *et al* 2003; Yang *et al* 2007), etc. Recently, Cheng *et al* (2011) successfully synthesized SnO_2 nanowires with diameters ranging from 20 to 200 nm through a polymeric sol–gel approach followed by a post-annealing in a crucible covered with a lid. All these above-mentioned methods are generally either of high cost or, to some extent, complicated. And, we can't totally handle all the chemical reactions in the process synthesizing SnO_2 nanowires. These drawbacks may limit the massive fabrication of SnO_2 nanowires and applications of these methods.

In this report a new option of SnO_2 nanowires fabrication method has been investigated. Large quantities of SnO_2 nanowires could be synthesized by a simple thermite reaction using Sn powder as the source material without adding any extraneous catalysts. In contrast with the above-mentioned methods, this method has obvious advantages. For example, it is a low cost, one-step, simple and easy. Also it doesn't require complex apparatus, sophisticated techniques, any extraneous catalysts, or templates as usually needed in other methods. And it is easy to control morphology of the resulting nanowires. In addition, there is high feasibility for a massive production of the nanowires via this method. Structural and optoelectronic properties of the as-synthesized SnO_2 nanowires are then examined by X-ray diffraction (XRD), scanning electron microscopy (SEM), transmission electron microscopy (TEM), X-ray photoelectron spectroscopy (XPS), Raman scattering and Fourier transform infrared spectroscopy. Furthermore, the growth mechanisms of these SnO_2 nanowires are also discussed.

*Author for correspondence (yznian@163.com)

2. Experimental

2.1 *SnO_2 nanowires synthesis*

SnO_2 nanowires were prepared based on the following reactions:

$$Al_{(s)} + CuO_{(s)} \rightarrow Al_2O_3 + Cu + \text{heat}, \quad (1)$$

$$Sn_{(S)} + \text{heat} \rightarrow Sn_{(l)}, \quad (2)$$

$$Sn_{(l)} + O_2 \rightarrow SnO_{2(S)}. \quad (3)$$

The synthetic process can be generalized into two procedures. During the first procedure, Al deoxidized CuO into Cu to release a large amount of heat. And then the Sn was melted immediately by heat and sprayed out of the reaction system. Once the molten Sn was exposed to air, oxidation took place.

We designed 3 reaction experiments, A, B and C, as shown in table 1. All the chemical reagents were dried by vacuum low temperature drying process. Experiment A is the basic experiment with a reaction system consisting of Sn (m_a g, 200 mesh, AR) powders, CuO (m_{Cu} g, 200 mesh, AR) powders and Al (m_a g, 200 mesh, AR) powders. O_2 was introduced to promote oxidation of the molten Sn in experiment B. CaO was introduced to moderate the violence of the reaction in experiment C, which was not the key element to growth of 1D nanostructures. All the chemical reagents were fully mixed as the rate shown in table 1.

The schematic drawing of the experiment, equipments and concrete experimental operating steps, is shown in figure 1.

Table 1. Compositions of three reaction systems for synthesizing SnO_2 nanowires by thermite reaction.

Experiments	Constituents (g)				Powder size (mesh)	Purity level	Reaction atmosphere
	Al	Sn	CuO	CaO			
A	m_a	m_s	m_{Cu}	–	200	Analytical reagent	Air
B	m_a	m_s	m_{Cu}	–	200	Analytical reagent	O_2
C	m_a	m_s	m_{Cu}	m_{ca}	200	Analytical reagent	O_2

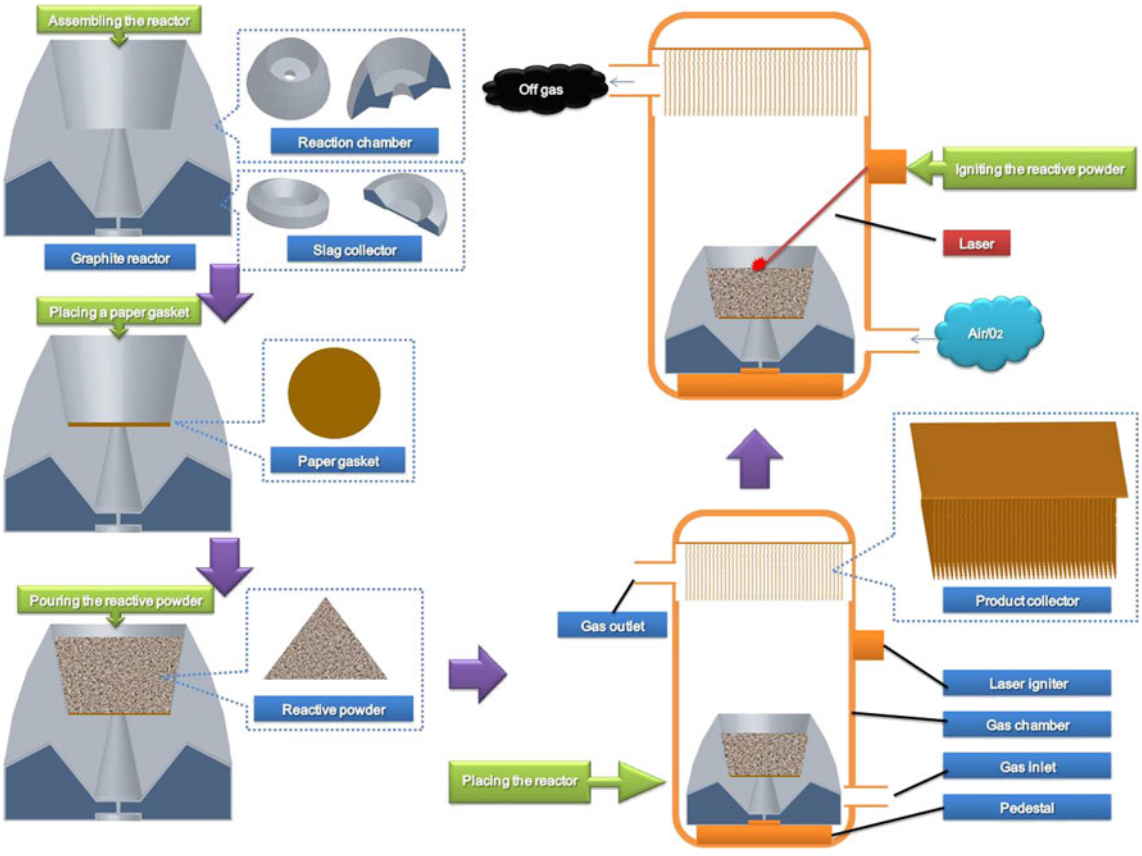

Figure 1. Processes of SnO_2 nanowires synthesis.

The graphite reactor consists of a reaction chamber, a bowl-shaped graphite vessel with a hole in the bottom, and a slag collector. And the product collector is a heat-resistant stainless steel plate array, placed on top of the gas pressure furnace before experiment, as shown in figure 1. A paper gasket was placed in the bottom of the reaction chamber to cover the hole before experiment, which was burned in the reaction to let the reaction residue drip into the slag collector under the reaction chamber. And after this, the mixed chemical reagents were poured into the reaction chamber and then placed into the gas pressure furnace within graphite reactor. Lastly, the mixed chemical reagents were ignited in the gas pressure furnace by the laser igniting system at 200 °C in air/O_2 atmosphere, in accordance with table 1, with a gas pressure of 0·9 atm. When the reaction finished, SnO_2 nanowires could be found on the surfaces of the product collector. It was found that these heat-resistant stainless steel plates were covered with a thick layer of gray cotton-like matter. And these SnO_2 nanowires were removed by brush and collected for characterization.

2.2 *Instrumentation*

X-ray diffraction (XRD) test was performed on an XRD diffractometer (D8-Advance, Bruker). The XRD patterns with CuK_α radiation ($\lambda = 0{\cdot}154$ nm) at 40 kV and 50 mA were recorded in the region of 2θ from 5 to 40°. Scanning electron micrographs (SEM) were taken on a Hitachi S-570 scanning electron microscope with 20 kV accelerating voltage and at a magnification of 3000. The elemental composition of the as-synthesized product was determined by an EDAX genesis 7000 energy dispersive spectroscopy (EDS) system operated at 20 kV. EDS system utilizes characteristic X-ray photons produced by the primary electron beam to probe chemical elements. The samples were examined using a JEM-2010HT transmission electron microscope (TEM) system equipped with a selected-area electron diffraction (SAED) attachment operated at 200 kV and a JEOL 2010FEF (UHR) microscope operated at 200 kV. X-ray photoelectron spectroscopy (XPS) was performed on a KRATOS XSAM800 X-ray photoelectron spectrometer, using MgKα radiation, with 16 mA current and 12 kV voltage (192 W), and a base pressure of 6×10^{-7} Pa in the sample chamber. Laser Raman spectrum was obtained using a Renishaw RM-1000 confocal laser microraman spectrometer from 100 to 1800 cm^{-1} at room temperature. The 514·5 nm line of the laser was used as excitation source, with the capability of supplying power less than 4 mW. PL measurements were performed using NICOLET 5700 Fourier transform infrared spectroscopy (FTIR) spectrometer equipped with an Continuum IR microscope.

3. Results and discussion

The phase composition and structure analysis of these as-synthesized products were carried out using X-ray diffraction. Figure 2 shows XRD patterns of the products of 3 experiments. All the peaks of patterns B and C can be well indexed to a tetragonal SnO_2 (ICDD-PDF72-1147, symmetrical group: *P*42/*mnm* (136)). In addition, any characteristic peak of Al, Al_2O_3, Cu, CuO, Sn and SnO, which is used or formed in the fabrication method, was not observed. Thus, the XRD result of product B and product C implies that the as-synthesized products were pure rutile SnO_2. Compared to patterns B and C, some characteristic peaks of Sn and SnO were observed in pattern A, which well indexed to Sn (ICDD-PDF85-0712) and SnO (ICDD-PDF65-0296). A careful comparison between the 3 experiments reveals that experiments B and C were carried out in O_2 atmosphere, while experiment A was carried out in air atmosphere. This observation combining with the XRD result indicates that the SnO_2 nanowires were formed out of the reaction chamber rather than inside it and adequate oxygen is necessary to get pure rutile SnO_2.

The morphology of the products of experiments B and C, which were dispersed by ultrasonic waves in anhydrous alcohol for 30 min before, were observed by TEM as shown in figures 3 and 4. It can be seen that the SnO_2 product of experiment B displays wire-like shape with a diameter of 80 nm and the SnO_2 products of experiment C had different sizes of globular particles with diameters in the range of 60–440 nm. This observation indicates that the SnO_2 products of experiment C were formed in different ways as compared to that of experiment B. Compared to experiments B and C, introduction of CaO to the reaction system contributed to the difference. To provide further insight into the detailed structure of SnO_2 nanowire in figure 3, its selected area electron diffraction (SAED) pattern was recorded with the electron beam along [−1 1 1] as shown in figure 5. From the SAED pattern, growth direction of the SnO_2 nanowire in figure 3 was found to be [1 0 1]. It also reveals that this SnO_2 nanowire is high quality single rutile crystals. Figure 6 shows HR–TEM image of another SnO_2 nanowire in the

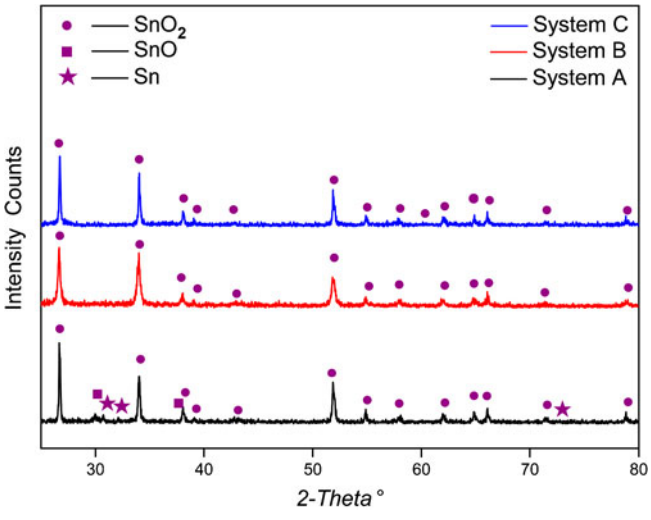

Figure 2. XRD patterns of products of 3 experiments.

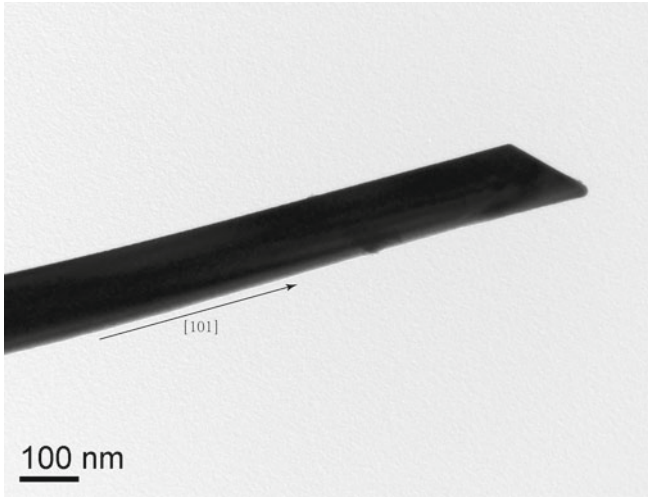

Figure 3. TEM image of one SnO_2 nanowire in product of experiment B.

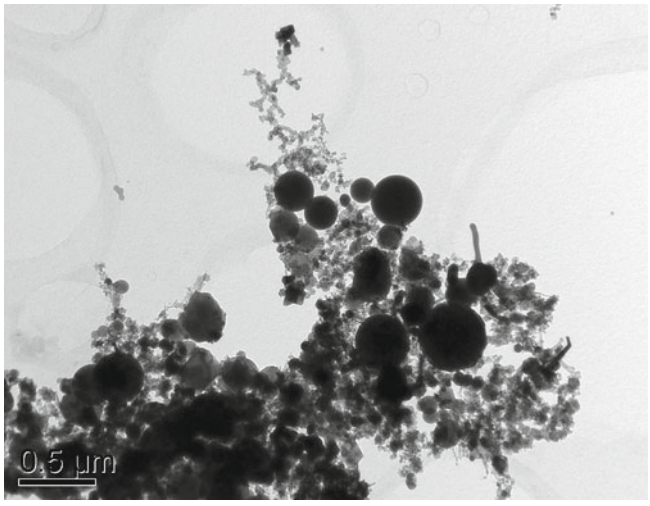

Figure 4. TEM image of product of experiment C.

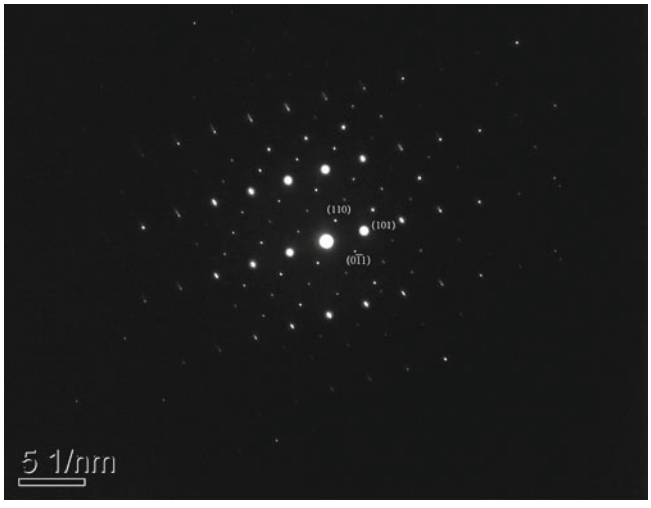

Figure 5. SAED pattern of SnO_2 nanowire in figure 3.

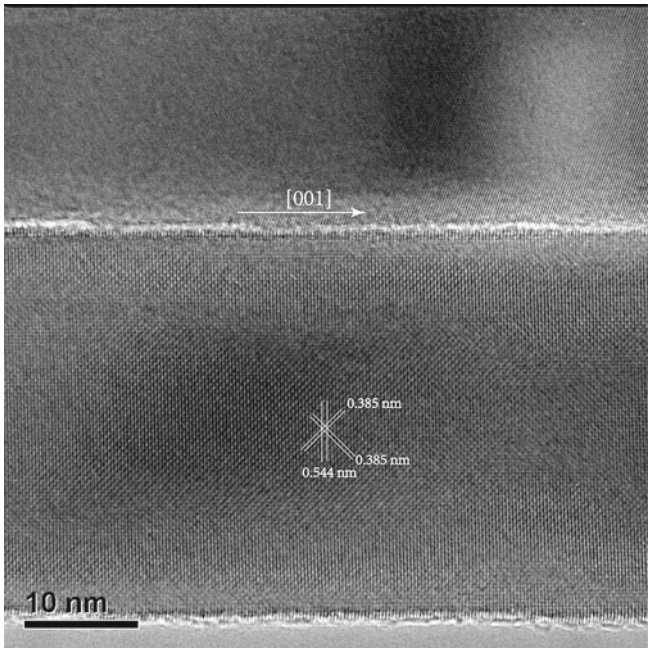

Figure 6. Lattice-resolved HR–TEM image of another SnO_2 nanowire in product of experiment B.

product of experiment B, with a diameter of 35 nm. HR–TEM image shows that the SnO_2 nanowire is structurally uniform and clear lattice fringes illustrate that the nanowire is a single crystalline with dislocation and point defects free. The interplanar spacing of the selected nanowire, which is about 0·385 and 0·544 nm, corresponds very well to {101} and {001} planes of the rutile crystalline SnO_2, respectively. It can be demonstrated further that this SnO_2 nanowire was growing along [001] direction, different from the growth direction of the SnO_2 nanowire in figure 3. It's worth noting that (110) crystal plane of tetragonal SnO_2 is thermodynamics sustained and it is nonpolar in [001] direction, so most of the one-dimensional SnO_2 nanocrystals are growing along [101], [200], or [301] direction rather than [001] direction. This observation suggests that there is some external power which overwhelms this barrier, allowing the SnO_2 nanocrystals to grow along [001]. Based on this analysis, we deduce that these SnO_2 nanocrystals of experiment B randomly grew in different directions within the constraints of some external power to form the as-grown nanowires.

Figure 7 shows SEM image of the SnO_2 nanowire products of experiment B, which were not dispersed by using ultrasonic waves. Our SEM analysis was performed over 100 nanowires to obtain the distribution shown in figure 7. SnO_2 nanowires are in the range of 20–100 nm in diameter and the mean diameter obtained from the distribution is about 60 nm, which is from the statistics on about five hundred nanowires on the same substrate. And they have lengths of several hundred micrometers, smooth and uniform along the fibre axis with some polyhedron particles located on their tip, which is different from that in figure 3. The reason for the difference could possibly be due to the fact that these polyhedron

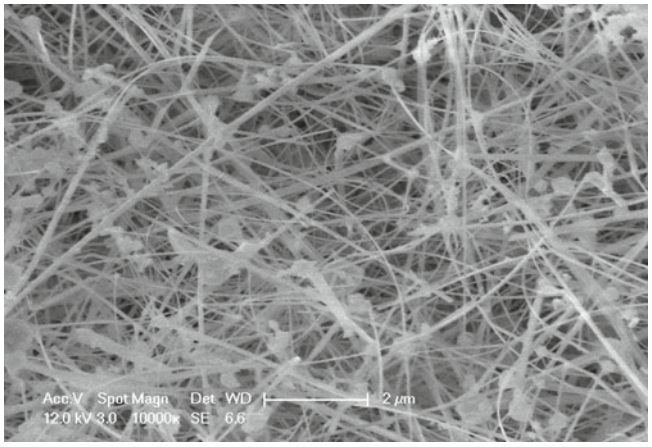

Figure 7. SEM image of SnO_2 nanowire products of experiment B, which were not dispersed by using ultrasonic waves.

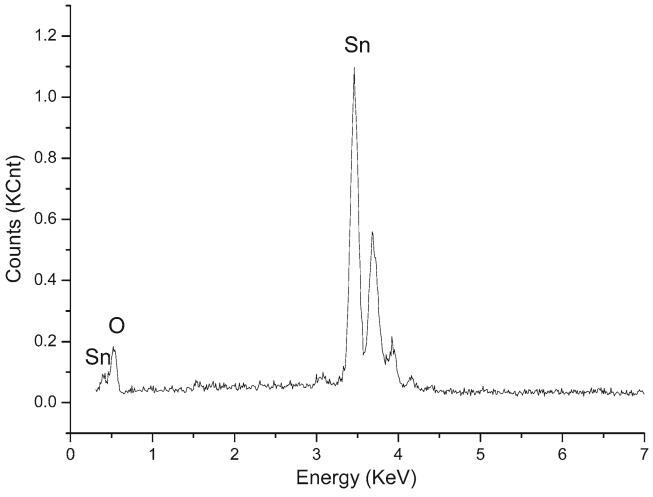

Figure 8. EDS analysis result of product of reaction system B.

particles fell off from the tip of the SnO_2 nanowires during ultrasonic dispersing process and were not collected by us. In the EDX spectrum depicted in figure 8, only peaks associated with Sn and O elements are present and any other Al or Cu related peaks are absent. The observation reveals that the SnO_2 nanowires are relatively pure and these polyhedron particles located on the tip of the SnO_2 nanowires were also SnO_2.

Combining the above analysis, the formation mechanism of SnO_2 nanowire products of experiment B in the present method is proposed as follows. As the reaction system was ignited, the combustion reactions would take place, according to (1)–(3). The calculation of free energy changes in these reactions were made using Gibbs–Helmholtz equation (4).

$$\Delta H = \sum \Delta H_{T_o} + \sum \int_{T_o}^{T_m} C_{P_1} \mathrm{d}T + \sum \Delta H_m + \sum \int_{T_m}^{T_e} C_{P_2} \mathrm{d}T, \quad (4)$$

where ΔH is the reaction heat, ΔH_{T_o} the enthalpy of product at the beginning temperature of reaction, C_{P_1} the heat capacity of product at temperature $T_o - T_m$ in pressure P, ΔH_m the melting enthalpy of product, C_{P_2} the heat capacity of product at temperature $T_m - T_e$ in pressure P, T_o the beginning temperature of reaction, T_m the melting point of product and T_e the highest temperature which the reaction system can reach to.

From the calculation, T_e obtained can be about 2296 K in experiments A and B and 2017 K in experiment C. In experiments A and B, T_m of product Al_2O_3 is 2327 K, T_m of product Sn is 505 K and T_m of product Cu is 1357 K. As the whole reaction system is a powder mixture, it can be seen as a compartmented box consisting of many tiny small molten pools. In a very tiny area of the reaction system A or B, the product Al_2O_3 is a porous solid on top of the reaction system, and liquid product Sn and Cu under it successively in the order of their density, as shown in figure 9. In experiment C, CaO combined with Al_2O_3 to form a eutectic crystal compound

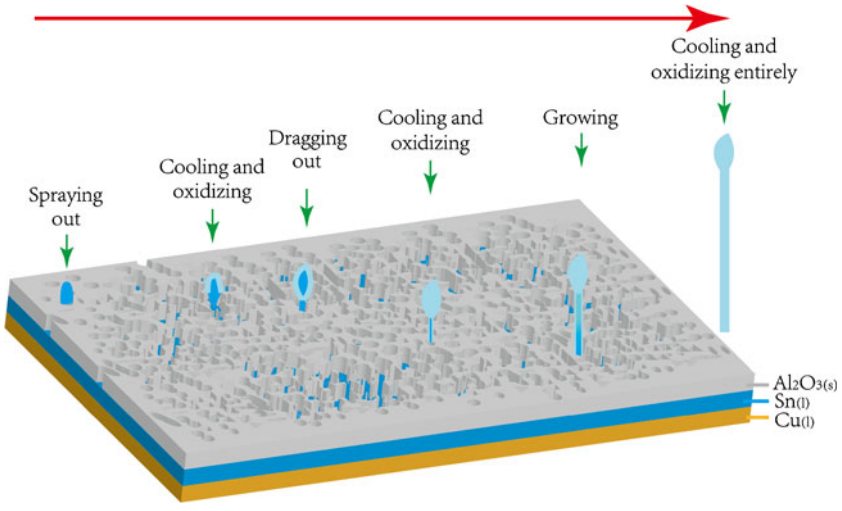

Figure 9. Growth process of SnO_2 nanowire products of experiment B.

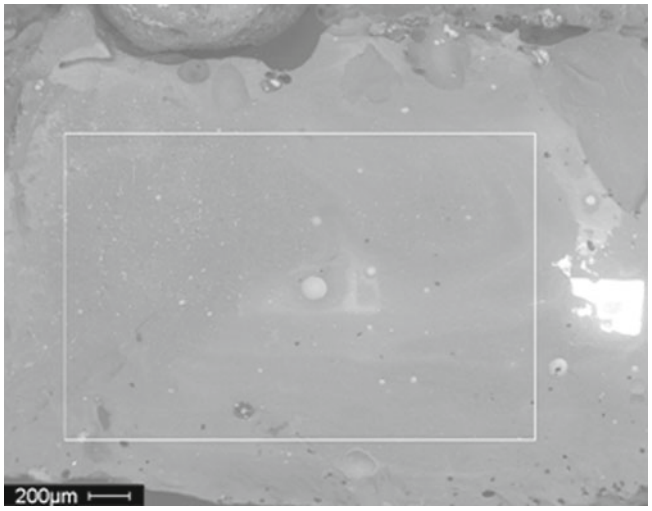

Figure 10. SEM image of $12CaO{\cdot}7Al_2O_3$ layer of experiment C.

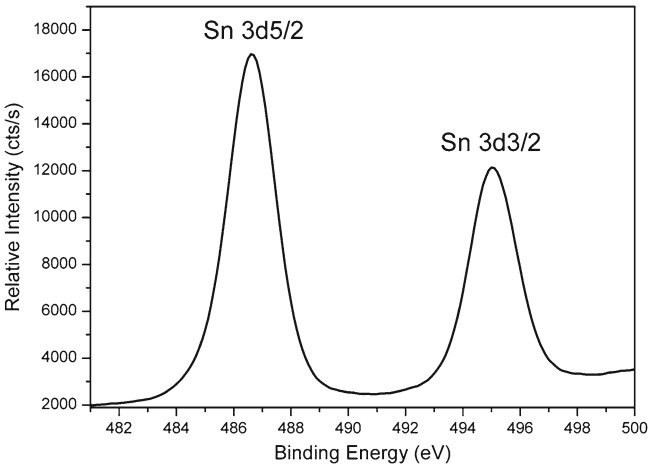

Figure 11. XPS spectrum of SnO_2 nanowire products of experiment B: Sn_{3d} core level.

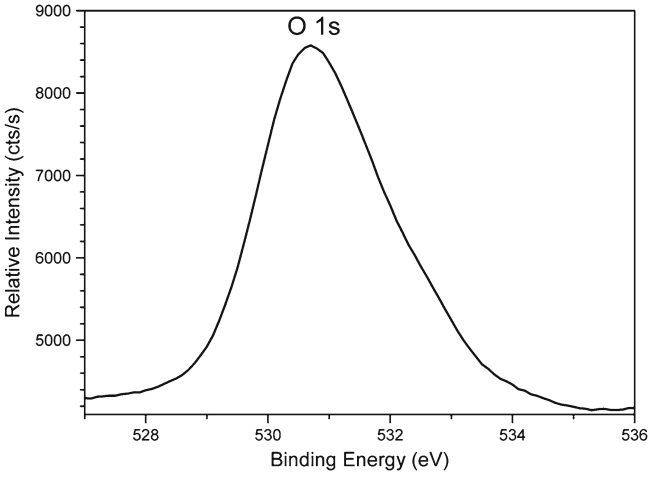

Figure 12. XPS spectrum of SnO_2 nanowire products of experiment B: O_{1s} core level.

$12CaO{\cdot}7Al_2O_3$ with a T_m below 2017 K. There is also no liquid product in experiment C. The same as the product Al_2O_3, $12CaO{\cdot}7Al_2O_3$ is a solid on the top of the reaction system, but with a dense structure rather than a porous structure, as shown in figure 10.

Figure 9 clearly shows growth process of the SnO_2 nanowire products of experiment B. In the beginning, melting Sn drop sprayed out from the micropore in porous Al_2O_3 scum and was oxidized and cooled immediately. The Sn drop sprayed upward continuously and dragged out the melting Sn adjacent to it. And then this melting Sn was dragged out from the micropore in porous Al_2O_3 scum to form a wire-like shape and was also oxidized and cooled immediately. As the nanowire grew, the dragging force died down. Eventually, the nanowire sprayed out entirely from the reaction chamber, and was cooled and oxidized into SnO_2. These SnO_2 nanowires grew randomly, so they did not grow in the same direction. This growth mechanism of SnO_2 nanowires can explain the reason why product of experiment A is not completely oxidized as that of experiment B. This is because air cannot oxidize all the sprayed melting Sn entirely. It also can explain the reason why product of experiment C is nanoparticle rather than nanowire which is because there is no porous Al_2O_3 scum on top of the reaction system as in experiment B, so that the melting Sn broke through the $12CaO{\cdot}7Al_2O_3$ layer and sprayed out without template constraint to form nanowire.

Figure 11 shows high-resolution XPS Sn3*d* of SnO_2 nanowire products of experiment B. Peaks at 486·6 and 495 eV corresponds to the binding energy of $Sn3d_{5/2}$ and $Sn3d_{3/2}$, respectively which are consistent with those observed in SnO_2 (Szuber *et al* 2001; Jaeyeong *et al* 2010; Li *et al* 2011). The binding energy of Sn $3d_{5/2}$ peak for stoichiometric SnO and SnO_2 is reported to be 486·3 and 487·3 eV, respectively (Szuber *et al* 2001; Li *et al* 2011). Figure 12 reveals XPS O1*s* of SnO_2 nanowire products of experiment B. The corresponding binding energy of O1*s* is 530·7 eV, which is also in agreement with datum obtained for SnO_2 (Szuber *et al* 2001; Jaeyeong *et al* 2010; Li *et al* 2011). XPS studies further confirm that SnO_2 nanowire products of experiment B are composed of pure SnO_2 and SnO. However, SnO content is so little that we cannot detect it by XRD. This composition makes it possible for some oxygen vacancies to form in these SnO_2 nanowires.

Rutile SnO_2 belongs to the point group D_{4h}^{14} and space group $P4_n/mnm$. Its normal lattice vibration at the Γ point of the Brillouin zone is given on the basis of group theory (Zhou *et al* 2006; Thanasanvorakun *et al* 2008; Cheng *et al* 2011):

$$\Gamma = 1A_{1g}+1A_{2g}+1A_{2u}+1B_{1g}+1B_{2g}+2B_{1u}+1E_g+3E_u.$$

Among them, A_{1g}, B_{1g}, B_{2g}, and E_g are allowed to Raman active modes. A_{2u} and E_u are allowed to IR active modes. A_{2g} and B_{1u} are inactive (Zhou *et al* 2006; Cheng *et al* 2011). Figure 13 shows room-temperature Raman spectrum of SnO_2 nanowire products of experiment B. It can be seen

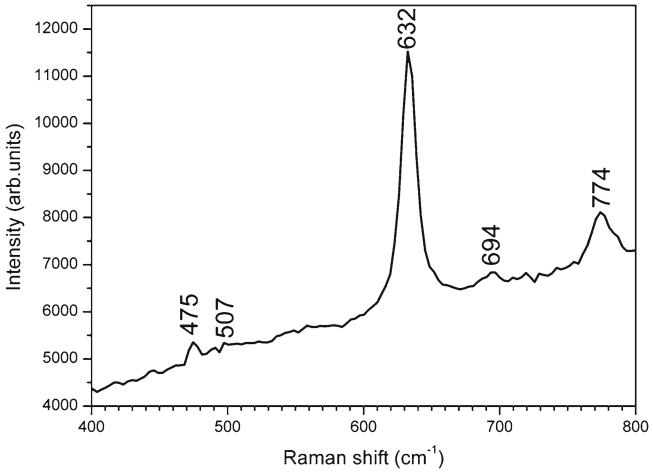

Figure 13. Raman scattering spectrum of SnO_2 nanowire products of experiment B.

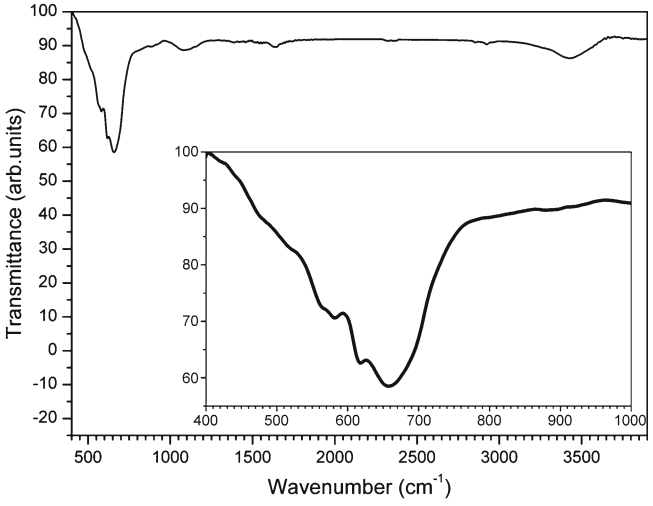

Figure 14. Mid-IR spectrum of SnO_2 nanowire products of experiment B.

that three fundamental Raman scattering peaks at 475, 632, and 774 cm^{-1}, respectively are in good agreement with those of a rutile SnO_2 nanowire single crystal (Wang *et al* 2002, 2004). The peak at 478 cm^{-1} can be identified as the E_g mode, peak at 632 cm^{-1} can be assigned to the A_{1g} mode, and peak at 774 cm^{-1} can be indexed to the B_{2g} mode. Raman spectrum again confirms that the SnO_2 nanowires have typical feature of the rutile phase of SnO_2. However, it is noteworthy that the 3 peaks become wider and there is downwards shift of the 3 peaks, compared with the SnO_2 powders, which is due to the nanosize effect of the nanowire (Jong-Soo *et al* 2004; Park *et al* 2007; Yang *et al* 2007). The peaks at 507 and 694 cm^{-1} seem to correspond to IR active A_{2u} symmetry with TO and LO modes, the appearance of which is possible because some IR active modes will loose their IR activity and become Raman active in nanocrystalline phase (Zhou *et al* 2006; Cheng *et al* 2011). To further explore the 2 peaks, these SnO_2 nanowires were also

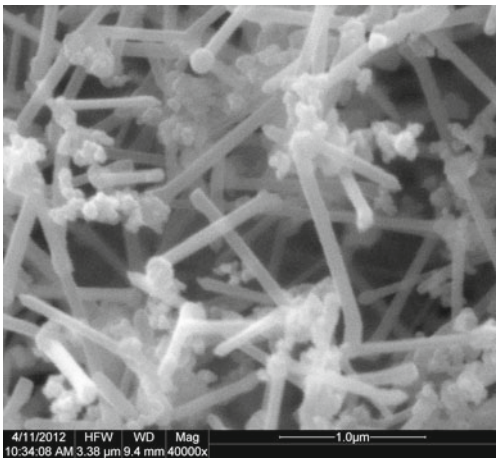

Figure 15. SEM image of ZnO nanowires synthesize via our method with similar reaction system, which weren't dispersed by using ultrasonic waves.

investigated by the mid-IR spectroscopy, as a complementary to the above mentioned details of SnO_2 microstructure experimental method. However, the two moulds are not obvious in figure 13. It is difficult to explain this phenomenon well in this paper. As shown in figure 14, the main variable peaks appear in the range of 400–800 cm^{-1}, which can be ascribed to the Sn–O lattice vibration of SnO_2 (Suhua *et al* 2006; Cheng *et al* 2011).

In addition, our method applies equally well to synthesize other metal oxides (1D) nanostructures, such as ZnO nanowires, SiO_2 nanowires, AgO nanowires and so on. Figure 15 shows the SEM image of the ZnO nanowires synthesize via our method with similar reaction system, which weren't dispersed by using ultrasonic waves. However, there are still many problems needed to be solved and more research is on the way.

4. Conclusions

In summary, a typical thermite reaction has been developed to synthesize highly yielded and uniform SnO_2 nanowires. High purity single-crystalline SnO_2 nanowires have been synthesized through one-step process at 200 °C in O_2 atmosphere, with a gas pressure of 0·9 atm. The as-prepared nanowires have diameters ranging from 20 to 100 nm and lengths extending to hundreds of micrometers and do not grow in one direction as that synthesized by other methods. They are perfect single crystals with rutile structure, without any dislocation or point defects detected in TEM images. Nevertheless, result of XPS analysis shows that some oxygen vacancies exist in them. In addition to three fundamental vibrational modes, E_g, A_{1g}, and B_{2g} two IR active modes are observed in the Raman scattering spectrum of SnO_2 nanowires. However, the two moulds are not obvious in their mid-IR spectrum. It is difficult to explain this phenomenon well in this paper. In comparison to the growth mechanism of

SnO_2 nanowires synthesized by some other methods, growth mechanism of SnO_2 nanowires prepared via our method is quite different. Sn was melted by the reaction heat, sprayed out from the micropore in porous Al_2O_3 scum, and was cooled and oxidized into SnO_2 by O_2. During the process, the Sn drop sprayed upward and dragged out the melting Sn adjacent to it so that it can form into a wire-like shape eventually. This method requires neither complex apparatus nor sophisticated techniques. It is hoped that it will be extended as a general method for synthesizing nano-oxides.

Acknowledgements

This work was supported by the Natural Science Foundation of Hubei Province (No. 2009CDB300), and the Fundamental Research Funds for the Central Universities of China (No. 5082001).

References

Ahmad A and Walsh J 2003 *J. Mater. Sci.* **38** 4325
Bhise A B, Late D J, Sathe B, More M A, Mulla I S, Pillai V K and Joag D S 2010 *J. Exp. Nanosci.* **5** 527
Budak S, Miao G X, Zdemir M O, Chetry K B and Gupta A 2006 *J. Cryst. Growth* **291** 405
Calestani D, Zha M, Zappettini A, Lazzarini L, Salviati G, Zanotti L and Sberveglieri G 2005 *Mater. Sci. Eng. C* **25** 625
Chen Y Q, Cui X F, Zhang K, Pan D Y, Zhang S Y, Wang B and Hou J G 2003 *Chem. Phys. Lett.* **369** 16
Cheng B C, Xie C C, Fang L T, Xiao Y H and Lei S J 2011 *Mater. Chem. Phys.* **129** 713
Dmitriev S, Lilach Y, Button B, Moskovits M and Kolmakov A 2007 *Nanotechnology* **18** 0557071
Francisco H R, Joan D P, Albert T, Sven B, Olga C, Roman J D, Eva P, Jordi R, Joan R M, Miguel A J, Sanjay M and Albert R R 2008 *Adv. Funct. Mater.* **18** 2990
Gubbala S, Chakrapani V, Kumar V and Mahendra K S 2008 *Adv. Funct. Mater.* **18** 2411
Huang J, Lu A X, Zhao B and Wan Q 2007 *Appl. Phys. Lett.* **91** 0731021
Ito S, Yamada Y, Kuze M, Tabata K and Yashima T 2004 *J. Mater. Sci.* **39** 5853
Jaeyeong H, Adam S H, Roy G G 2010 *Chem. Mater.* **22** 4964
Jang H S, Kang S O and Kim Y I 2006 *Solid State Commun.* **140** 495
Jian J K, Chen X L, Wang W J, Dai L and Xu Y P 2003 *Appl. Phys. A* **76** 291
Jin Z Q, Ding Y and Wang Z L 2005 *J. Appl. Phys.* **97** 0743091
Jong-Soo L, Sung-Kyu S, Byungdon M, Kyoungah C, Soo Won K and Sangsig K 2004 *J. Cryst. Growth* **267** 145
Kang K S and Lee S P 2003 *J. Mater. Sci.* **38** 4319
Li C C, Yin X M, Li Q H and Wang T H 2011 *Cryst. Eng. Comm.* **13** 1557
Liu R B, Chen Y J, Wang F F, Cao L, Pana A L, Yang G Z, Wang T H and Zou B S 2007 *Physica E* **39** 223
Luo S H, Fan J Y, Liu W L, Zhang M, Song Z T, Lin C L, Wu X L and Chu P K 2006 *Nanotechnology* **17** 1695
Ma Y J, Zhou F, Lu L and Zhang Z 2004 *Solid State Commun.* **130** 313
Mazzone A M 2007 *Solid State Commun.* **143** 481
Park M S, Wang G X, Kang Y M, Wexler D, Dou S X and Liu H K 2007 *Angew. Chem. Int. Ed.* **46** 750
Pijolat C, Riviere B, Kamionka M, Viricelle J P and Breuil P 2003 *J. Mater. Sci.* **38** 4333
Qu D M, Yan P X, Chang J B, Yan D, Liu J Z, Yue G H, Zhuo R F and Feng H T 2007 *Mater. Lett.* **61** 2255
Salviati G, Lazzarini L, Zha M Z, Grillo Vincenzo and Carlino Elvio 2005 *Phys. Status Solidi (a)* **202** 2963
Suhua L, Paul K C, Weili L, Miao Z and Chenglu L 2006 *Appl. Phys. Lett.* **88** 1831121
Szuber J, Czempik G, Larciprete R, Koziej D and Adamowicz B 2001 *Thin Solid Films* **391** 198
Tae-Hwan J, Soon-Il K, Jae-Hwan P, Dong-Gun L, Young-Jin C and Jae-Gwan P 2008 *Appl. Phys. A* **91** 707
Thanasanvorakun S, Mangkorntong P, Choopun S and Mangkorntong N 2008 *Ceram. Int.* **34** 1127
Wan Q, Dattoli E N and Lu W 2007 *Appl. Phys. Lett.* **90** 2221071
Wang W Z, Xu C K, Wang G H, Liu Y K and Zheng C L 2002 *J. Appl. Phys.* **92** 2740
Wang J X *et al* 2004 *Solid State Commun.* **130** 89
Wang W Z, Niu J Z and Ao L 2008 *J. Cryst. Growth* **310** 351
Yang M R, Chu S Y and Chang R C 2007 *Sensor Actuat. B: Chem.* **122** 269
Ying Z, Wana Q, Cao H, Song Z T and Feng S L 2005 *Appl. Phys. Lett.* **87** 1131081
Zhou J X, Zhang M S, Hong J M and Yin Z 2006 *Solid State Commun.* **138** 242